SYMPOSIUM 1990
BELGRADE YUGOSLAVIA

15

FLOW SURVEY AND BLADE PRESSURE MEASUREMENTS IN A FRANCIS TURBINE MODEL

SONDAGES D'ECOULEMENT ET MESURES DE PRESSION D'AUBAGE DANS UN MODELE DE TURBINE FRANCIS

François Avellan, Philippe Dupont, Mohamed Farhat, Bernard Gindroz, Pierre Henry, Mahmood Hussain, Etienne Parkinson, Olivier Santal

EPFL, Institut de Machines Hydrauliques et de Mécanique des Fluides
avenue de Cour, 33, CH 1007 Lausanne, Switzerland

SUMMARY

Experimental flow analysis of hydraulic machines is of prime importance for improving the design of such a unit. Moreover, computational fluid dynamics codes need an experimental data reference in order to check their ability to simulate the main flow features. To obtain such an experimental data base a Francis turbine model and an associated instrumentation is specially developed. Measurements of both global and local quantities are performed for five different operating points of the turbine. A five-hole probe mounted on a remote displacement system provides static pressure and velocity components along three stations in the machine. An original rotating instrumentation is implemented in order to obtain the pressure distribution over the blades of the runner at 28 points (17 on the suction side and 11 on the pressure side) arranged along three streamlines.

RESUME

L'analyse expérimentale des écoulements dans les machines hydrauliques est d'une importance primordiale dans l'amélioration du tracé de ces unités. De plus, les codes de calculs d'écoulement ont besoin de données expérimentales de référence afin de vérifier leur capacité dans la simulation correcte des principales propriétés de l'écoulement. Pour construire une telle base de données expérimentale un modèle d'une turbine Francis et l'instrumentation qui lui est associée sont spécialement développés. Les mesures des variables à la fois globales et locales sont effectuées pour cinq points de fonctionnement de la turbine. Une sonde de pression à cinq trous installée sur un système de déplacement automatique permet de relever la pression statique et les trois composantes de la vitesse le long de trois axes de sondages dans la machine. Un équipement original de mesure de pression embarqué dans la roue fournit la distribution de pression sur les aubes de la roue en 28 points (17 à l'extrados et 11 à l'intrados) distribués le long de trois lignes de courant .

INTRODUCTION

Flow analysis in hydraulic machines is of prime importance for improving the design of these units. As is usual in hydraulic science, both numerical simulations and experimental flow survey are performed in order to investigate the local flow properties such as a low pressure region or a strong adverse pressure gradient on the blades. Moreover, flow analysis can provide, from the planning stage of a new machine, an estimate of the head losses of each component of the turbine, and an accurate prediction of the optimum operating point. The IMHEF Computational Fluid Dynamics Research Group has developed an incompressible Euler code well suited to the complex geometry of a Francis turbine runner, see [1]. In order to check the ability of this code to simulate the flow in this type of turbine, IMHEF has designed a full experimental set-up. A research model of a Francis turbine with medium-high specific speed was built with special features such as an adjustable stayring, probe passages and pressure taps on the stationary parts. The runner is equipped with pressure transducers in order to measure the pressure distribution on the blades. The detailed results obtained for the best operating point during tests carried out on the IMHEF Universal Hydraulic Machine Test Facility [2] were used at "the Gesellschaft für Angewandk Mathematik und Mechanik" workshop on the computation of incompressible internal flows as an experimental data reference [3]

The aim of this paper is to detail all the experimental set-ups in use for flow analysis of a Francis model. Special attention is paid to the design of both the flow survey instrumentation consisting of a five-hole probe mounted on a remote traversing system and the rotating pressure measurement. A few examples of the data obtained are provided for some of the five operating points investigated and finally the preliminary data analysis is described.

MODEL OF FRANCIS TURBINE

General design

The model to be tested corresponds to a Francis turbine of medium-high specific speed, $\nu = 0.5$, ($n_q = 76$). This model is especially designed for research purposes in order to perform experimental flow analysis. The spiral case is Piguet-type and is designed in order to have a constant meridional velocity distribution. Meridional sections of the spiral case are given in Figure 1. A fillet is added on both sides of the inlet of the stayring in order to provide the stayring with a well-defined inflow condition.

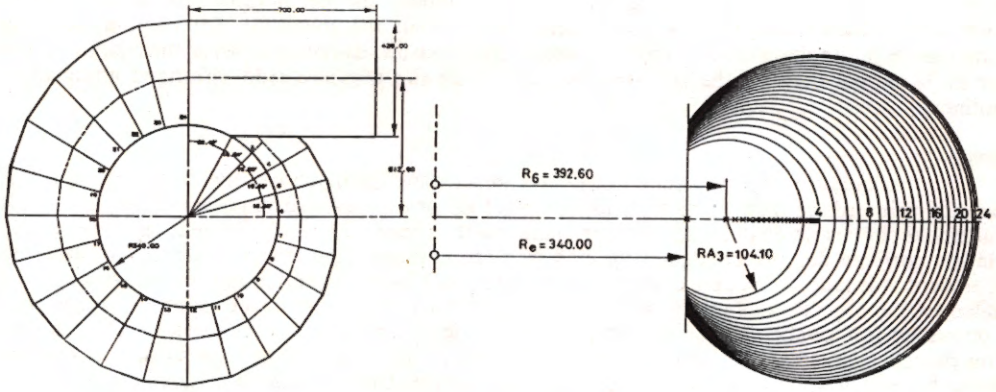

Figure 1 : Spiral case

The stayring is made of 24 stay vanes and the distributor of 24 guide vanes. The relative angular position of these two cascades can be adjusted but, in the case of the present study the angular positions, θ_d and θ_{ad}, remain unchanged and are set at 26.5° and 15° respectively, see Figure 2. A mechanical encoder provides a readout of the guide vane opening angle α. The opening angle α, is given in relation to the clearance opening in mm, Figure 3. Since the closed position of the guide vanes corresponds to $\alpha = 0$ and an angle $\gamma_d = 5.27$ °as indicated in Figure 2, the opening angle α is related to the guide vane angle as follows :

$$\gamma_d = \alpha + 5.27$$

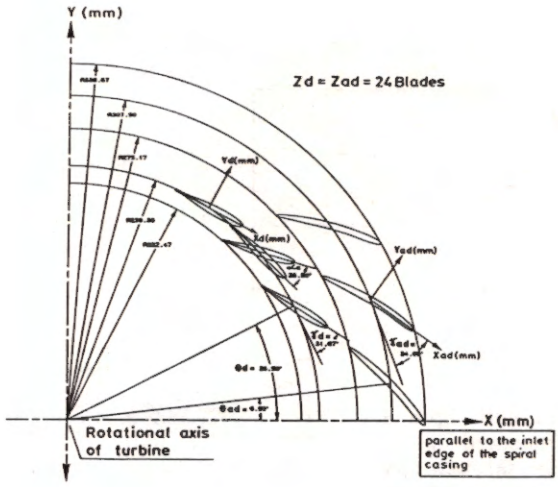

Figure 2 : Stayring and the distributor seen from above

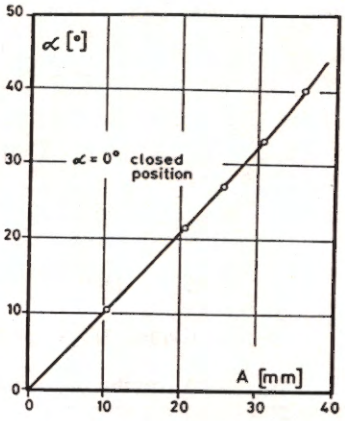

Figure 3 : Calibration curve of the guide vane opening angle

The runner is an IMHEF design with 13 blades, individually casted epoxy resin reinforced with carbon fiber, and fitted into an aluminium hub and shroud. The runner outlet diameter is 0.4 m. Cross-sections of both the pressure side and the suction side of the blade are given in Figure 4.

The draft tube used in this experimental study is not at all an up-to-date shape. It is designed to provide for numerical simulation work the simplified geometry of a cone, a constant section bend and an outlet cone without any inner pillar. The geometry of the draft tube is given in Figure 5.

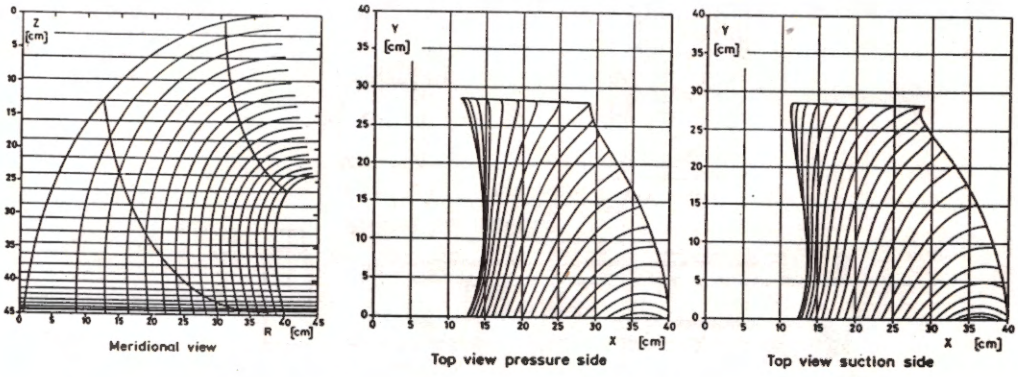

Figure 4 : Runner blade geometry

Flow survey system

Probe passages

More than 60 probe passages are made in the model in order to perform a flow survey at the distributor inlet, at the inlet and the outlet of the runner and in a cross-section of the cone.The location of these passages and the corresponding measurement axis are defined in Figure 6. A special mechanical arrangement allows these passages to be used either as a probe passage or a static pressure tap. Centering holes are drilled in the base plate of the model for a precise adjustment of the traversing system.

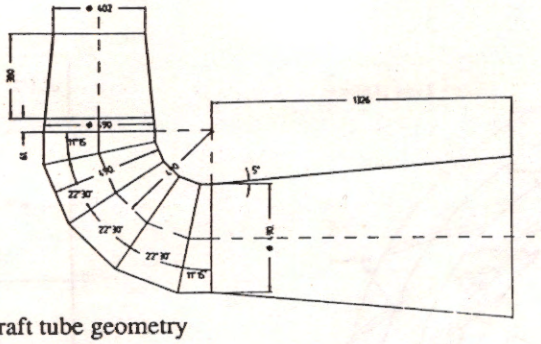

Figure 5 : Draft tube geometry

Remote traversing system

A remote traversing system with both a translatory and a rotatory positioning is mounted on the model base-plate in order to drive a probe through any passage of the model. The traversing system support is made of a rigid square light alloy tube, see Figure 7. The turntable providing the angular positioning is mounted in one end of the tube. The turntable is supported by a preloaded playless ball race and driven by a stepper motor with a worm and gear system. The linear motion is achieved with a stepper motor driven actuator mounted on the rotating part of the turntable and supported at the other end by a ball-bearing fitted in the squared tube support of the traversing system. The linear drive system incorporates a fixed lead screw and a moving nut where the probe support is mounted.

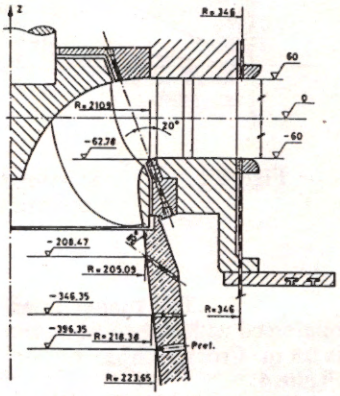

Figure 6 : Flow survey axes

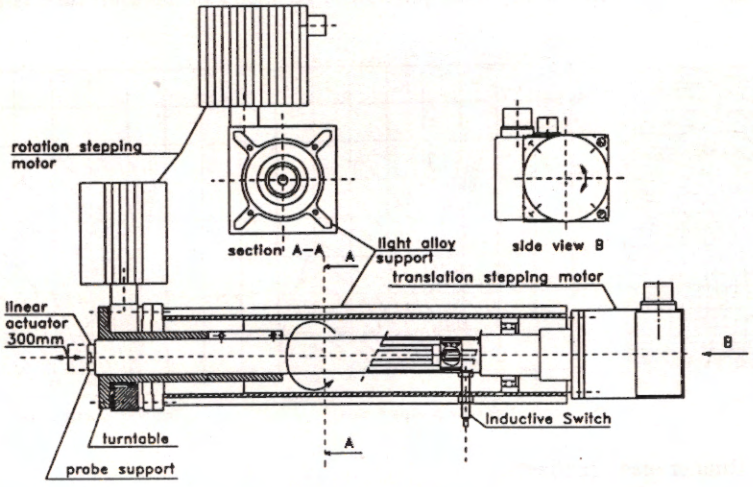

Figure 7 : Sketch of the traversing system

Both the relative linear and angular positions are numerically read by optical shaf encoders mounted on the stepper motor shafts. In order to define an accurate origin for each axis o motion, electronic logic gates are used firstly to rectify a contactless switch output and then to combine this output with the corresponding encoder signal output. The resulting signal is used tc permit the zero setting of the electronic counters, Figure 8. The two displacements can be done using

I5

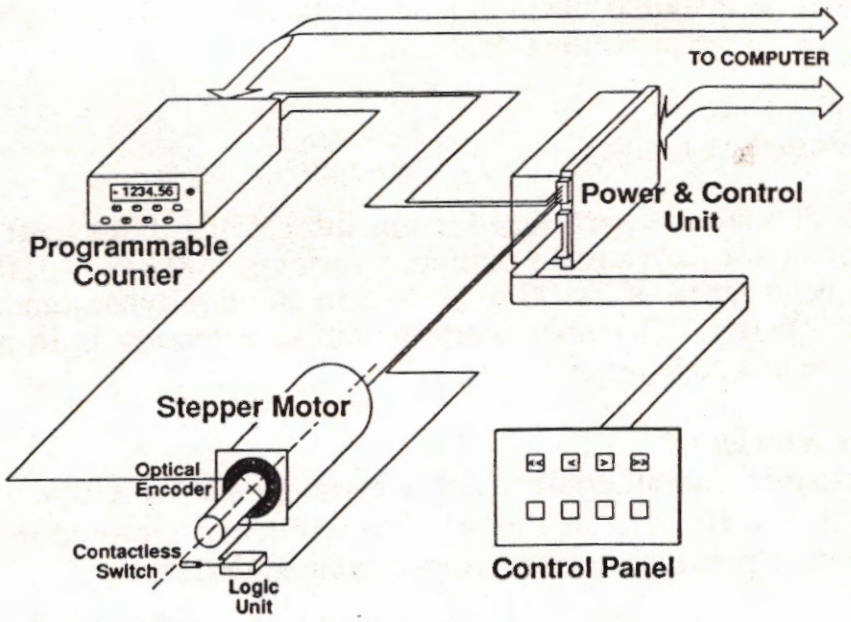

Figure 8 : Sketch of the traversing control units.

panel control command keys with a digital read out of the position, or through a remote-controlled microcomputer with an appropriate soft command.The sensitivity of one motor step corresponds to 6 10^{-6} m and 10^{-2} ° for the translation and the rotation respectively. An accuracy of less than ±20 10^{-6} m and ±.2 ° is achieved in the probe positioning. The linear positioning capacity is .3 m and the probe can be rotated through 360°.

Instrumented runner

Pressure transducers are mounted flush with the blade surface of the runner. The pressure transducers (resistive bridge) are fitted on the model of the blade during the casting process. The wires of each full bridge are embedded in the carbon fiber and epoxy resin material of the blades up to the hub of the runner. All the processing and the transmitting electronics are placed in the hub of the runner. The lead and signal wires pass through the hollow shaft up to the transmitting coil. By following this assembling process up to 3 transducers can be fitted on one blade, and then up to 28

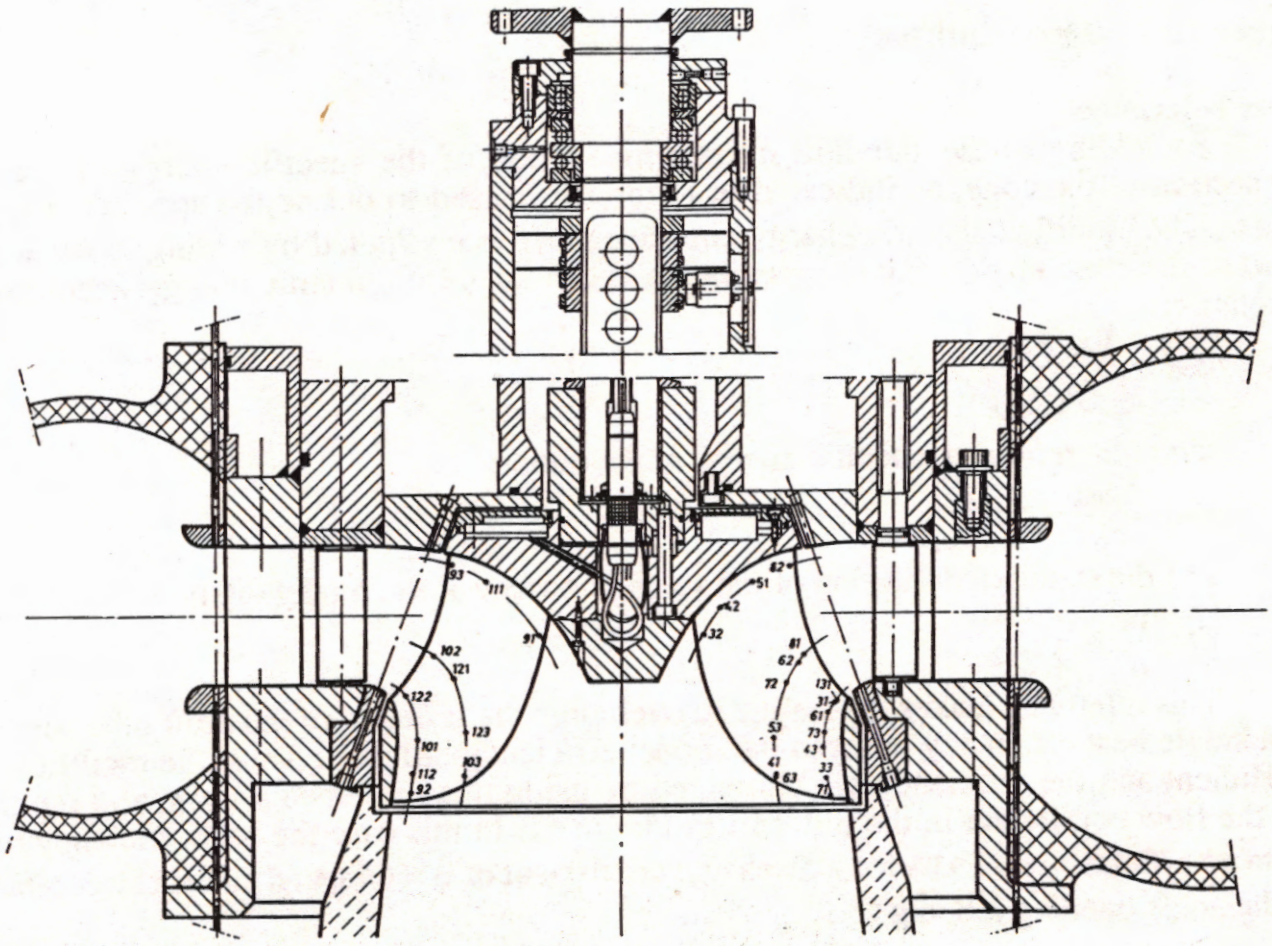

Figure 9 : Instrumented runner

15

pressure transducers can be installed on the blade surfaces, 17 of them are mounted on the suction side of the blades, and 11 on the pressure side, Figure 9.

PERFORMANCE TESTS

Universal machine test facility

The model tests are performed using the IMHEF Universal Hydraulic Machine Test Facility. Its main characteristics are a main pumping power of 900 kW at 1, 000 rpm, a maximum flow rate of 1.4 m³/s, a test head range of 2-100 m with a maximum dynamometer power of 300 kW at a maximum speed of 2'500 rpm. The test instrumentation accuracy is in accordance with the IEC turbine model acceptance test code requirements.

Hydraulic characteristics

The hydraulic characteristics for a given guide vane opening angle are given in a normalized φ–ψ form, Figure 10 . The model efficiency hillchart reported in the same figure presents two maxima due to the poor pressure recovery of the conical draft tube .

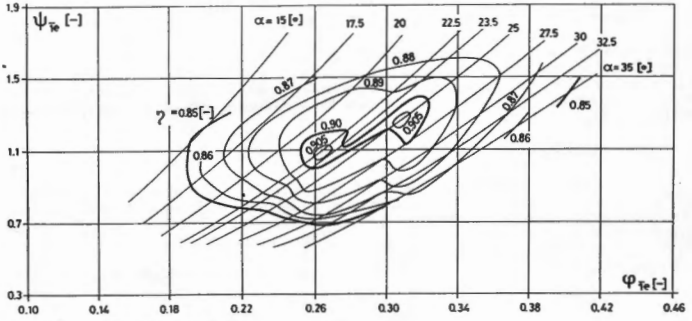

Figure 10 : Model hillchart

Cone reference

By adding to the standard measuring section of the specific energy of the model, a measuring section in the cone, as indicated in Figure 6, is used to define the specific energy at the runner outlet . The modified specific energy coefficient φ_{ref} is computed by adding to the wall static pressure p_{ref} at the cone station the corresponding mean specific dynamic energy according to the following relations:

$$\varphi_{ref} = \frac{E_I - E_{ref}}{\frac{1}{2}\omega^2(R_{Te})^2}$$

with the reference specific energy at the outlet:

$$E_{ref} = \frac{p_{ref}}{\rho} + \frac{1}{2}\frac{Q^2}{S_{ref}^2}$$

and the standard definition of the specific energy at the model inlet:

$$E_I = \frac{p_I}{\rho} + \frac{1}{2}\frac{Q^2}{S_I^2}$$

This reference makes it possible to overcome the problem of the draft tube behavior and to retrieve a single best efficiency point in the model efficiency hillchart. Thus, the modified specific energy coefficient and the efficiency are computed by using this reference station, and reported as a function of the flow coefficient in the hillchart in Figure 11. In this case the best efficiency operating point leads to an efficiency η of 93% for a discharge coefficient of $\varphi = 0.28$, and an energy coefficient of $\varphi_{ref} = 1.07$, the angle opening α being 25.5°.

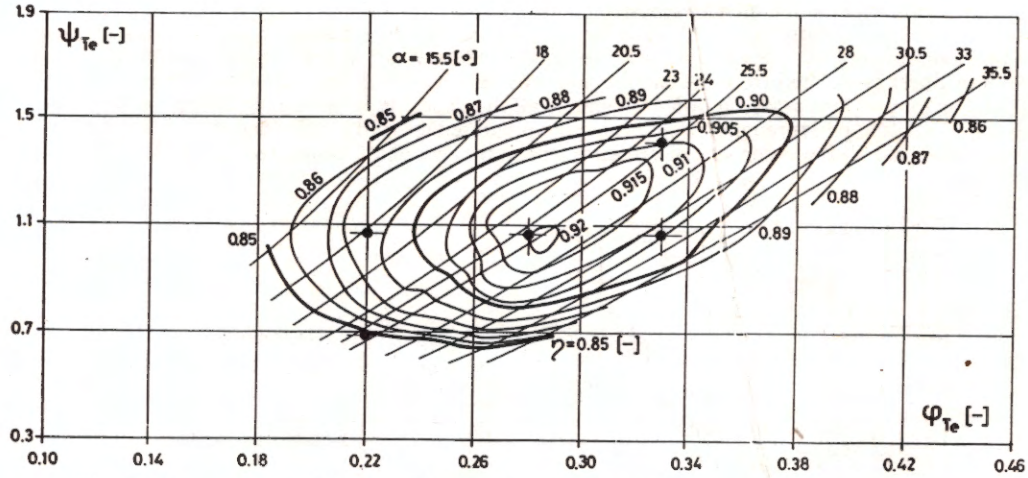

Figure 11 : Model hillchart with an outlet reference at the cone station

The simultaneous measurement of the specific energy of the whole model and of the model without the draft tube allows us to subtract the corresponding values in order to estimate the specific energy loss in the draft tube, Figure 12. Unfortunately, it does not lead to the exact draft tube losses, since an approximate specific kinetic energy term is used instead of integrating the actual flow kinetic energy in this station.

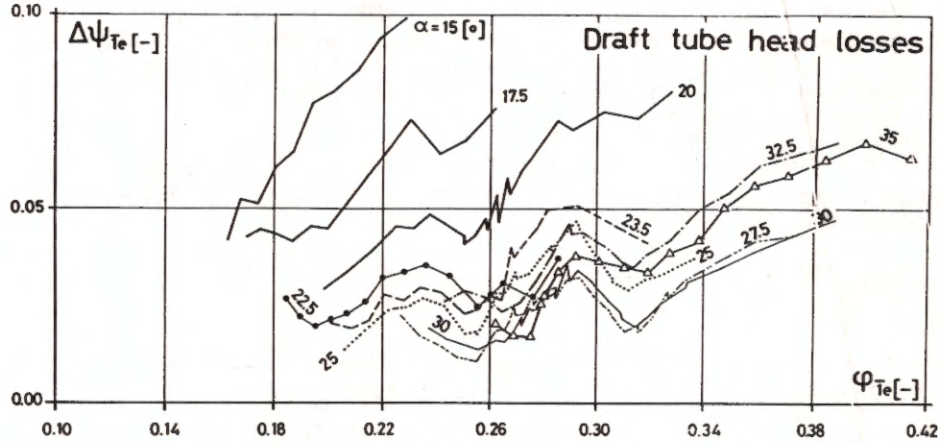

Figure 12 : Draft tube head losses

FLOW SURVEY INSTRUMENTATION

Five-hole probe

Design

The 6 mm diameter five-hole probe is designed to perform a full traversing survey of the flow in the different stations of interest by retrieving the 3 components of the local flow velocity and the local static pressure. The 0.5 mm diameter pressure tap arrangement is based on the one in the probe available from United Sensor, see Figure 13. In this case the probe is extended by a rod in order to guide it in the probe passages. The rod diameter is the same as the probe outer tube. The guiding bearings at the probe passages eliminate as far as possible the mechanical vibrations and allow the flow profile to be measured right across the flow channel for relevant head and flow values .

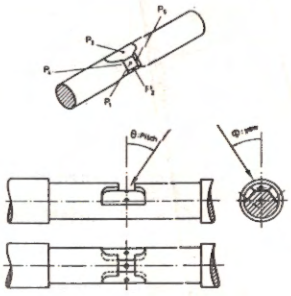

Figure 13 : Probe pressure tap arrangement

Static pressure measurements

Static pressures are measured by a water pressure line scanning system. This system, driven by a micro-computer uses two scanivalves connected to an absolute pressure transducer, Figure 14. The transducer is isolated from the facility water by silicone oil and an automatic drain procedure is followed as long as necessary, in order to remove all the undesirable bubbles in every pressure line. In addition to the five pressure taps of the probe, the pressure taps of the reference model inlet station, the cone station and all the other sets of pressure taps in the model are connected to the scanning line system.

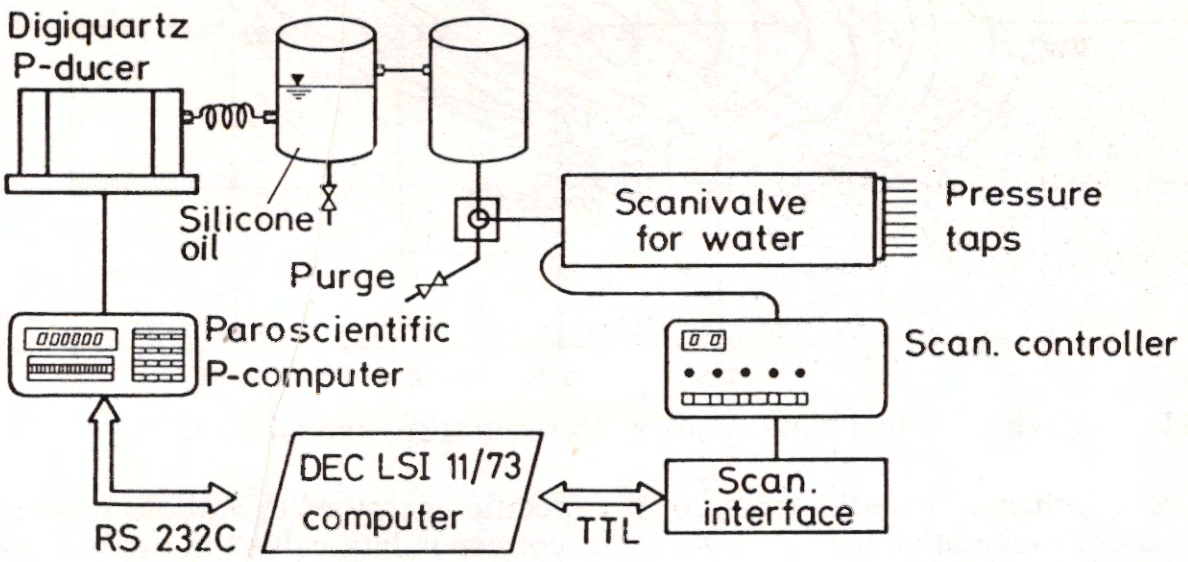

Figure 14 : Pressure line scanning system

Calibration

The probe is calibrated in the test section of the IMHEF High Speed Cavitation Tunnel. The absolute pressure measurements corresponding to the five holes are carried out for different pitch and yaw angles of the probe as a function of the flow velocity and the static pressure in the test section. If the set of five pressures p_1, p_2, p_3, p_4,and p_5 corresponds to the holes, Figure 13, we can define a mean pressure p_m as follows:

$$p_m = p_2 + p_3 + p_4 + p_5$$

With this definition, the following coefficients F and G are introduced as functions of the yaw angle ϕ and the pitch angle θ since the difference $p_1 - p_m$ behaves like a dynamic pressure in the range of the yaw angle of interest.

$$F(\phi,\theta) = \frac{p_2 - p_3}{p_1 - p_m} \qquad G(\phi,\theta) = \frac{p_4 - p_5}{p_1 - p_m}$$

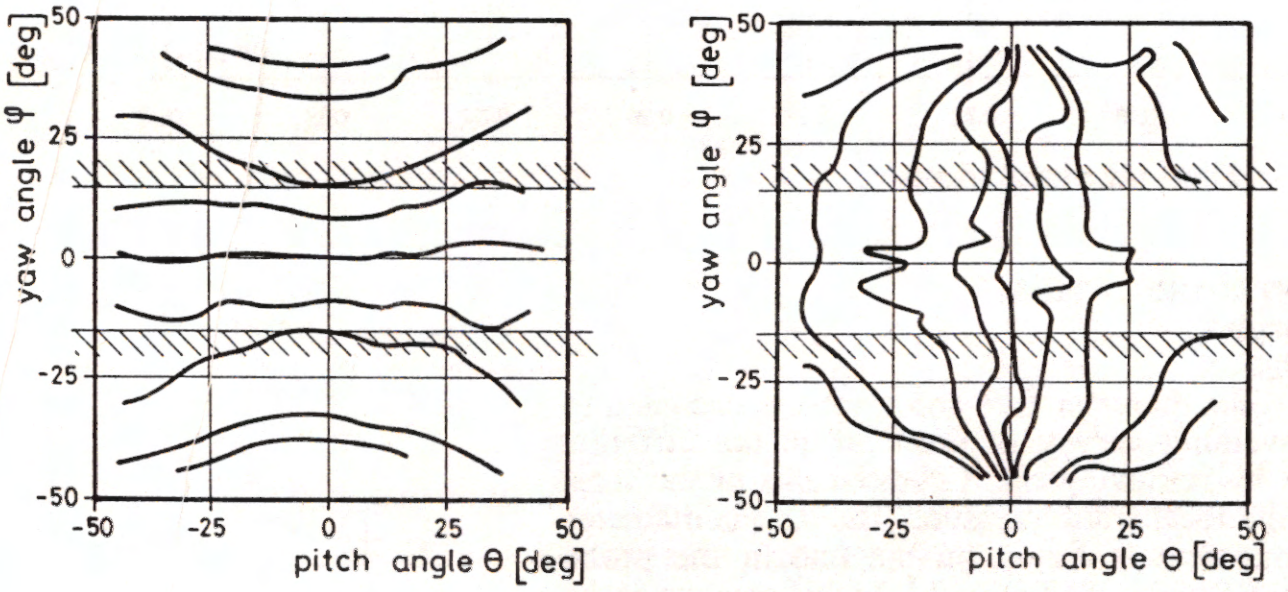

Figure 15 : Calibration surfaces of the yaw and pitch angles

I5

Calibration curves are given in Figure 15 as contoured surfaces of F and G values in a ϕ,θ map. It can be observed that F is most likely to be independent of θ and the G coefficient is independent of ϕ. In contrast to the F coefficient the G surface is not well-defined for the value of the yaw angle greater than 15° or smaller than -15°.
In addition a set of coefficients H and L, depending on the static pressure p_0 and the total pressure p_t, is plotted as a function of the flow angles, Figure 16.

$$H(\phi,\theta) = \frac{p_1 - p_m}{p_t - p_0} \qquad L(\phi,\theta) = \frac{p_1 - p_t}{p_t - p_0}$$

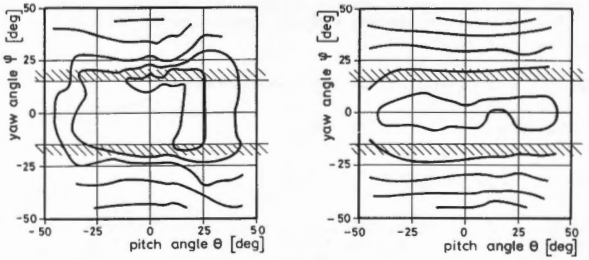

Figure 16 : Calibration surfaces of the total and static pressure

During the flow measurement procedure, these four surfaces make it possible to compute the F and G coefficients in order to find a corresponding pair of ϕ,θ angles. By getting the angle values the H and L coefficients are calculated, and in turn lead to the static and the total pressure. The velocity intensity C is then computed according to the definition of the dynamic pressure.

$$C = \sqrt{\frac{p_t - p_0}{\frac{1}{2}\rho}}$$

Flow measurement

The probe being calibrated is mounted at the end of the linear actuator of the traversing system. The displacement origins are set using the switch references. The five probe pressures and pressures at the reference inlet and at the cone reference station are measured sequentially. The flow angles are determined, and if the the yaw angle ϕ is not within a range of ±15°, the probe is rotated in order to be in the specified range and to achieve good accuracy for the flow velocity. The flow angle, the velocity intensity and static pressure are computed in the model frame of reference according to the definition in Figure 17 .

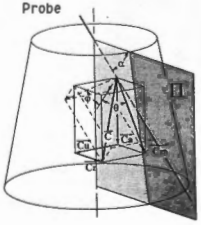

$$\begin{bmatrix} C_r \\ C_\theta \\ C_x \end{bmatrix} = \begin{bmatrix} C_r \\ C_u \\ -C_a \end{bmatrix} = C \begin{bmatrix} \cos\alpha & 0 & -\sin\alpha \\ 0 & 1 & 0 \\ \sin\alpha & 0 & \cos\alpha \end{bmatrix} \cdot \begin{bmatrix} \cos\theta\cos\phi \\ \cos\theta\sin\phi \\ \sin\theta \end{bmatrix}$$

where in this case α is the angle of the probe axis with the runner rotation axis.

Figure 17 : Velocity component in the probe frame of reference

In order to overcome any drift of the test facility operation the actual static and total pressures are scaled by a kinetic energy term as follows:

$$Cp_{o(probe)} = \frac{p0 - pref}{pI - pref} \qquad Cp_{t(probe)} = \frac{pt - pref}{pI - pref}$$

Even though the actual flow rate value cannot be sampled simultaneously with the probe pressure measurement, this scaling of the pressure, related to the reference pressure using a value similar to a kinetic energy term, allows us to compare successfully the measurements carried out for different test heads. These coefficients are then related to the reference dynamic pressure provided by the test rig data. For instance, the static pressure coefficient Cp_o is computed according to :

$$Cp_o = Cp_{o(probe)} \frac{pI - pref}{\frac{1}{2}\rho\omega^2(R_{Te})^2}$$

This leads to the following definition of the velocity coefficient c:

$$c = \frac{C}{U_{Te}} = \frac{C}{\omega R_{Te}}$$

PRESSURE MEASUREMENTS IN THE RUNNER

The miniature absolute pressure transducers fitted in the runner blades are of a resistive bridge type model PS-2KA from Kyowa. Their diameter and thickness are 5 mm and 0.6 mm respectively. The pressure range is 2 10^5 Pa and the mean sensitivity 900 µV/V.

The multiplexed bridge signal is voltage to frequency converted in order to be transmitted trough a coil mounted on the rotating shaft. The stationary part of the electronics consists of a receiving coil and a numerical counter driven through a serial interface by the microcomputer, Figure 18.

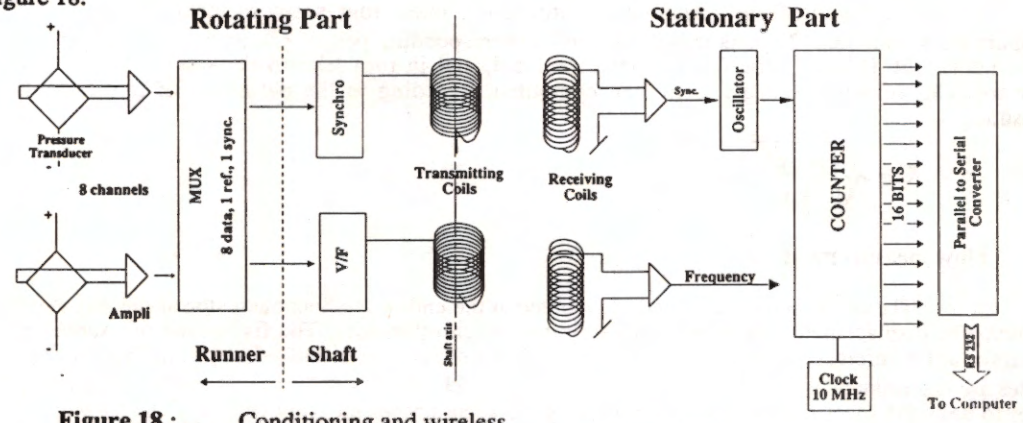

Figure 18 : Conditioning and wireless transmitting electronics

When runner is at rest, the pressure transducer is calibrated by varying the static pressure of the test rig, Figure 19. The pressure distribution is obtained for a given operating point by scanning the 28 pressure transducers. The data is reduced by computing the time average of the pressure signal corresponding to the nth transducer and scaled as follows:

$$Cp_k = \frac{pk - pref}{pI - pref}$$

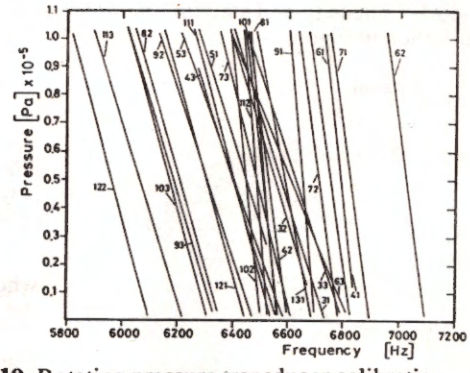

Figure 19 :Rotating pressure transducer calibration

I5

RESULTS

Operating points

The operating points investigated in this study are given in the hillcharts in Figures 10 and 11. They are chosen in order to vary only one of the operating parameters around the best efficiency operating point ; three of them have the same specific energy, and three have the same guide vane opening. The corresponding opening angles of this set of 5 operating points are given in the following table:

ψ \ φ	0.22	0.28	0.33
1.40	--------	--------	25.5°
1.07	19.5°	25.5 °	33.0°
0.66	25.5°	--------	--------

Flow survey

An example of flow survey at the runner outlet is given in Figure 20. The three diagrams correspond to the same ψ and to three flow coefficients. Unfortunately probe vibrations due to the low flow regime instability, $\varphi = 0.22$, prevent the core part of the flow to be crossed. Inversion of the tangential component c_u is observed as long as the flow rate is increased. The radial distribution of the tangential component, c_u, starts from a positive (unstable) solid rotation distribution at low flow to reach a free vortex distribution at high flow with an inverse rotation. Moreover, during this high flow regime, viscous diffusion leads to an in inverse solid rotation development in the core of the flow up to a normalized radius of 0.07. At the best efficiency operating point the tangential velocity tends to follow the distribution specified by the blade trailing edge angle in the outer part, r/R_{1e} greater than 0.4. The axial component distribution is not uniform in any flow regime, even at the duty point where a flow defect is observed in the central part. This low axial velocity region corresponds to the wake of the runner hub. At the high flow regime the maximum axial velocity falls to a normalized radius of 0.12. In this high axial velocity region, a deviation of the flow in both directions tends to render the axial velocity distribution uniform. This deviation is made apparent by the radial component of the velocity being negative in the inner core and positive at the periphery. The positive value of the radial velocity component close to the wall corresponds to the cone divergence. The static pressure distribution is uniform even though in a high flow region a low pressure in the core leads to predicting the onset of a whirl cavity.

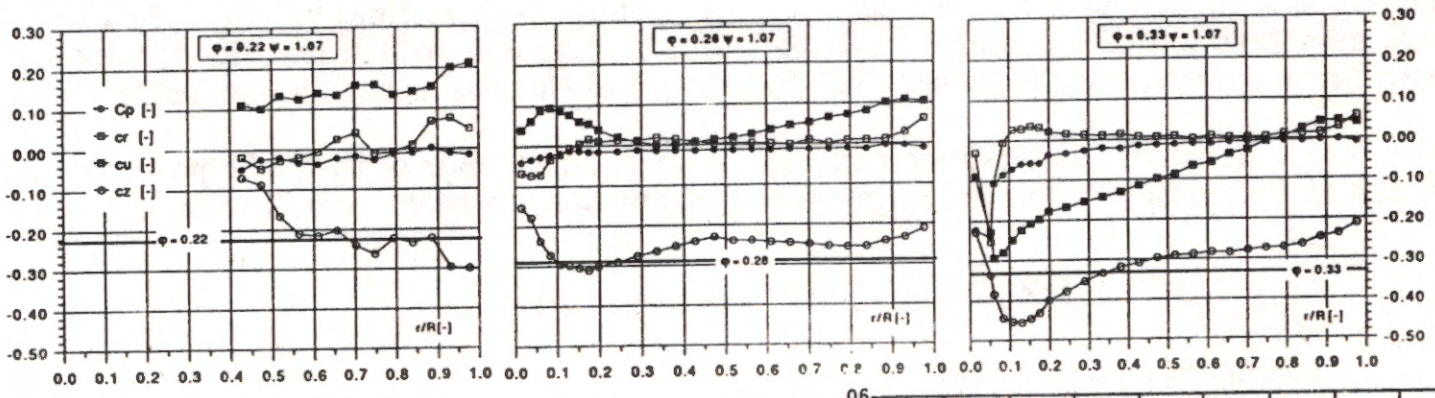

Figure 20 : Flow survey at the runner outlet

Pressure distribution in the runner

The pressure coefficient distribution along three streamlines close to the hub and the shroud, and corresponding to a midspan position is given in Figure 21. These values show that even at the best efficiency point the blade loading is far from being optimized. Low pressure distribution takes place close to the shroud leading to a possible inlet cavity development at the leading edge. Moreover the strong adverse pressure gradient could lead to a possible flow separation.

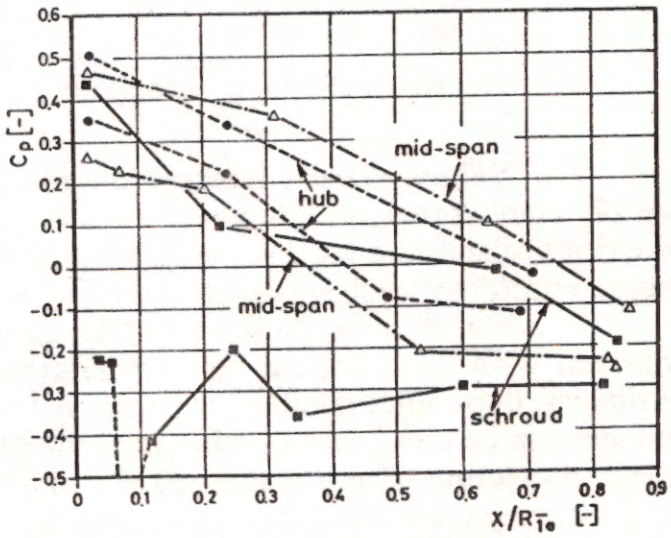

Figure 21 : Blade pressure distribution

Local variable integration

Both the local velocity and static pressure distribution in different sections allow a balance of convected flow properties to be carried out. For an incompressible flow the conservation of mass leads to the definition of the flow rate Q .

$$Q = \int_S \vec{C} \cdot \vec{n} dS$$

or by introducing the normalized quantities:

$$\varphi = \frac{1}{2\pi} \int_S \vec{c} \cdot \vec{n} ds$$

where S is the area corresponding to the section of interest. Integration of these relations allows the accuracy of the velocity measurements to be checked. Results are reported in Figure 21 as a function of the φ value provided by the test rig flowmeter. Depending on the station, a shift of the integrated value is observed, the values integrated at the outlet of the runner being the most underestimated. This can be due to the unsteadiness of the flow in this section.

Integration of the mean angular momentum about the rotation axis leads to an estimate of the net torque acting on the volume of fluid,V, under consideration This estimate then takes the following form :

$$\int_{SI}^{SII} (\vec{R} \times \rho \vec{C}) \vec{C} \cdot \vec{n} dS = \sum_V \vec{T}$$

Where SI, SII, are the limiting outlet and inlet sections of the volume of fluid V. The use of normalized variables gives :

$$\frac{1}{2\pi} \int_{SI}^{SII} (\vec{r} \times \vec{c}) \vec{c} \cdot \vec{n} ds = \sum_V \frac{\vec{T}}{\frac{1}{2}\rho\pi\omega^2 (R_{1e})^5}$$

According to the notations, the axial component of this equation leads to

$$\frac{1}{2\pi} \int_{SI}^{SII} r \cdot c_u \, \vec{c} \cdot \vec{n} ds = \sum_V \frac{T}{\frac{1}{2}\rho\pi\omega^2 (R_{1e})^5}$$

The resulting torque is integrated either on the fluid volume limited at the inlet by the spiral case-stayring section, or by the guide-vane runner section, the outlet section being in both cases the runner-cone section. The corresponding net torque acting on these fluid volumes are quoted in Figure 22 as a function of the normalized shaft torque measured by the test rig dynamometer. Obviously the integrated torque is greater since friction is included in this angular momentum balance

Similarly, the conservation of energy leads to an estimate of hydraulic power losses in the each part of the model. The integral form of this conservation law takes the following form :

$$\int_{SI}^{SII} [p + \frac{1}{2}\rho \vec{C}^2 + \rho g Z] \vec{C} \cdot \vec{n} dS = \sum_V \text{hydraulic power losses}$$

and in normalized variables:

$$\frac{1}{2\pi} \int_{SI}^{SII} [Cp + \vec{c}^2 + \frac{gZ}{\frac{1}{2}\omega^2 (R_{1e})^2}] \vec{c} \cdot \vec{n} ds = \sum_V \text{normalized power losses}$$

Values of these integrals are reported as function of the hydraulic power coefficient λ in Figure 22. They correspond to power transformation between the inlet of the stayring, the runner inlet and the draft tube outlet section., and the cone section as outlet section in all cases. Since these power balances are referred to the cone section, the loss in the draft tube appears to be negative.

For all these global balances the lack of accuracy of the flow velocity prevents a direct comparison with the standard test rig data being made, mainly in the case of low flow regimes. Nevertheless, these integrated values are consistent with each other. The relative losses of each turbine component can be computed in relation to the power transformation (100 %) between the stayring inlet and the cone section. These values are added and plotted in Figure 23 in order to compare them to the model efficiency related to the cone section. These losses are presented in two sets of operating points, constant guide vane opening and constant specific energy coefficient respectively, as a function of the

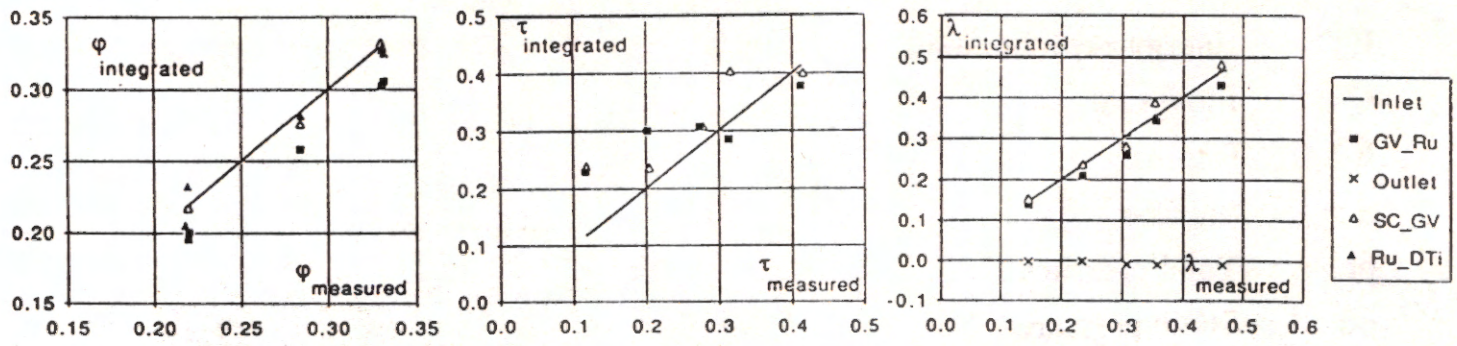

Figure 22 : Local variable integration

flow coefficient. These values agree well with the efficiency excepted at the low flow regime and low head. Obviously the minimum power losses take place at the best operating point.

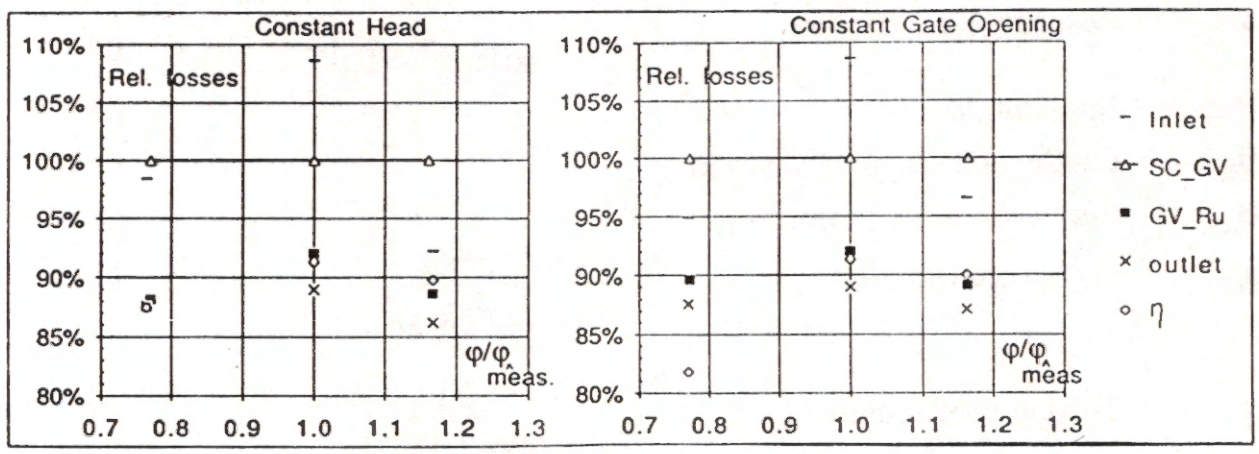

Figure 23 : Relative power losses in the model

CONCLUSIONS

A complete experimental set-up is developed in order to perform a flow analysis in a model of a Francis turbine. Measurements of both global and local quantities are performed for five different operating points of the turbine. A five-hole probe mounted on a remote displacement system provides static pressure and velocity components along three stations in the machine, and an original rotating instrumentation is installed in order to obtain the pressure distribution on the blades along three streamlines. This flow survey in the model allows the distribution of power losses in each component of the turbine to be investigated. Even though the accuracy of local velocity measurements is far from being of the same order as the global parameters provided by the test rig instrumentation, a balance of angular momentum and power can be obtained leading to a meaningful power loss estimate. This experimental procedure is essential for improving of our knowledge of the inflow condition of hydraulic machines .

ACKNOWLEDGEMENT

The authors wish to thank all their colleagues from the Technical Staff of the IMHEF Test Rig. This work is supported financially by Sulzer Escher Wyss and Vevey Engineering Works.

NOTATIONS

E :	Energy per mass unit		$[J \cdot kg^{-1}]$
Q :	Flow rate		$[m^3 \cdot s^{-1}]$
R :	Radius		[m]
S :	Surface		$[m^3]$
pt :	Total pressure		[Pa]
p :	Static pressure		[Pa]
α :	Guide vane opening		[°]
ϕ :	Yaw angle		[°]
γ_d :	Guide vane closed position angle		[°]
φ :	Discharge coefficient	$\frac{Q}{\pi(R_{\tilde{1}e})^2 (2E)^{1/2}}$	[-]
θ :	Pitch angle		[°]
θ_d :	Guide vane angular position		[°]
θ_{ad} :	Stay vane angular position		[°]
λ :	Power coefficient	$\frac{2EQ}{\pi\omega^3(R_{\tilde{1}e})^5}$	[-]
τ :	Torque coefficient	$\frac{2T}{\rho\pi\omega^2(R_{\tilde{1}e})^5}$	[-]
υ :	Specific speed	$\frac{\omega(Q/\pi)^{1/2}}{(2E)^{3/4}}$	[-]
ρ :	Density		$[kg \cdot m^{-3}]$
ω :	Angular speed		$[rad \cdot s^{-1}]$
ψ :	Energy coefficient	$\frac{2E}{\omega^2(R_{\tilde{1}e})^2}$	[-]

REFERENCES

[1] Thibaud F., Drotz A., Sottas G., 1988, "Validation of an Euler code for hydraulic turbines", *Proceedings of the AGARD Symposium, La validation du calcul en dynamique des fluides*, 2-5 mai 1988, Lisbonne, Portugal.

[2] Henry P., 1985, "Hydraulic machine model acceptance tests", *Proceedings of International Conference on Hydropower, Water Power '85*, Las Vegas, vol. 2, pp. 1258-1267.

[3] *Proceedings of the GAMM Workshop*, 1989, Lausanne, to be published by *Vieweg Verlag* in the series *Notes on Numerical Fluid Mechanics*